PIV-UQ database description

This document describes the PIV-UQ database that can be downloaded on the web page www.piv.de/uncertainty. The database is intended to be publicly available for the general use of the research community for development, evaluation and benchmarking of PIV-UQ methods. Furthermore, these data can be used in the development of PIV processing and post-processing methods, particularly those used in TR-PIV.

The database comprises the raw images, from which the velocity fields can be measured, and the reference velocity, which is the "exact" velocity measured with a more accurate PIV system. The measurement error can thus be computed as the difference between measured velocity and reference velocity, and used to assess the accuracy of PIV-UQ methods.

Some of the data contained in the database have been published in Neal *et al* (2015).

1. Experimental setup[1]

The experiments were conducted in the Experimental Fluid Dynamics Laboratory (EFDL) at Utah State University, where the rectangular jet used by Timmins *et al* (2012) and Wilson and Smith (2013) is operated. The jet facility has a rectangular nozzle of aspect ratio 7.2, based on a width w = 72.8 mm and a height h = 10.2 mm. The measurements were conducted at jet exit velocity u_0 = 5 m/s, which yields a Reynolds number based on the jet height of approximately 3,000. The data were acquired at various sampling rates in the range 4-10 kHz.

The flow was seeded with a Rocket Portable Smoke System (model #PS23 - 1.1 kW) that uses a glycerine-water solution as working fluid and produces droplets with 1 μm median diameter. The illumination source was a Photonics Industries laser (model DM40-527) with pulse energy of 40 mJ at 1 kHz. The laser light sheet thickness was set to 1.7 mm and measured by traversing a photodiode.

Two PIV systems acquired images simultaneously in time-series mode: these are named measurement system (MS) and high dynamic range (HDR) system.

1.1. PIV measurement system: PIV-MS

The PIV-MS is based on a single camera that records time-resolved (TR-PIV) images of the particle tracers. The system yields the velocity components within the illuminated plane (2D-2C PIV). A LaVision HighSpeedStar 5 (CMOS, 10 bit, 1024×1024 pixels, 17 μm pixel pitch, 3000 frames per second at full resolution) was equipped with a Nikkor 105 mm focal length lens set to $f\#$ = 4. The optical magnification of the system was 0.122, leading to a digital imaging resolution of 7.2 px/mm. The typical size of the particle images was about 1.5 px and was regulated by slightly shifting the focal plane of the camera.

1.2. PIV high dynamic range system: PIV-HDR

The PIV-HDR system was a two camera time-resolved (TR-PIV) system that could measure 3 components of velocity over a nominally 2D light sheet. The two cameras were LaVision

[1] Further details on the experimental setup are reported in Neal *et al* (2015)

HighSpeedStar 6 (CMOS, 12 bit, 1024×1024 pixels, 20 μm pixel pitch, 5400 frames per second at full resolution) in a stereoscopic configuration (SPIV). Camera #1 was normal to the laser sheet and mounted a Nikkor objective of 105 mm focal length set to *f*# = 5.6. Camera #2 had an angle of 49 degrees with respect to the laser sheet normal and used a Nikkor 200 mm focal length lens set to *f*# = 5.6. This specific stereo configuration allows for the HDR system to be used either as a 2D-2C PIV system (using only camera #1) or as a SPIV system (using both cameras). The optical magnification was 0.535, leading to a digital imaging resolution of 26.7 px/mm. The optimal particle image diameter of 2.5-3 px (Raffel *et al*, 2007) was achieved by slightly defocusing the images. Note that the PIV-HDR system had a larger digital imaging resolution by about factor 3.7 with respect to the PIV-MS. As a result, a particle image displacement in the physical space is discretized by a larger number of pixels in the image space for the PIV-HDR system than for the PIV-MS. Hence, since the measurement error is approximately independent of the measured displacement, the PIV-HDR system yields lower relative error by about factor 3-4.

1.3. PIV-HDR data processing

The PIV-HDR recordings have been processed with the LaVision DaVis 8.1.6 software. The HDR system employed the sliding-average correlation algorithm (Sciacchitano *et al*, 2012) on a kernel of five image pairs to further reduce the measurement error. The final interrogation window size was 32×32 pixels, corresponding to a measurement region of 1.42 mm × 1.42 mm. The overlap factor was set to 87%. Spurious vectors were detected with the universal outlier detection approach (Westerweel and Scarano, 2005), which removed and replaced via linear interpolation of neighboring vectors. No smoothing of the data was performed neither in space nor in time.

2. Velocity field

The time-averaged velocity and fluctuations root-mean-square of the jet flow are reported in figure 1. The jet begins in the laminar regime ($x/h = 0$) and shear layer instabilities start at $x/h > 4$, causing a rapid increase of the flow fluctuations. The largest velocity fluctuations occur at $x/h \approx 8$ due to the pairing of spanwise vortices. For $x/h > 10$, the flow is in the turbulent regime.

A series of experiments were carried out in different regions of the rectangular jet. Specific locations were targeted where the flow features pose challenges for the PIV measurements, as illustrated in figure 1-b. The resulting datasets form a benchmark database with numerous test cases for evaluating PIV uncertainty and advanced PIV processing algorithms. The measurement regions include:

a) Steady inviscid jet core and laminar shear layer ($x/h \approx 1$)

The jet core region is characterized by steady potential flow. The seeding density was varied within the range {0.3, 0.9, 1.8, 3.0 particles/mm^3}. The numerical aperture of the PIV-MS system was also varied (*f*# = {2.8, 4, 5.6, 8}) throughout the tests. The latter parameter is important to study the effect of varying the particle image diameter in relation to the peak-locking effect.
Within the shear layer close to the jet exit the flow is still steady, but the velocity gradient has an important component across the shear layer. Under these conditions, the measurement errors can be dominated by the effect of particle pattern deformation as well as by the lack of spatial resolution.

b) Unsteady inviscid jet core and vortex roll-up region ($x/h \approx 4$)

In this region, a pulsatile motion of the core flow is inducted by the Kelvin-Helmholtz vortices that bound the region. This results in an inviscid unsteady flow, with low-frequency velocity fluctuations.

Beyond the stable region of the free shear layer, the growth of Kelvin-Helmholtz vortices introduces large fluctuations of both the streamwise and transverse velocity components. The flow remains laminar with a quasi-sinusoidal behavior in the transverse component. The instantaneous streamline curvature induced by such effects becomes significant.

e) Developed jet turbulence (x/h = 19 and y/h = 0, -0.4, -0.5)

Downstream of the collapse of the potential core, the jet undergoes transition to the turbulent regime. Here the velocity field features more isotropic fluctuations and out-of-plane motion of the particle tracers. The latter, however, remains relatively small when compared to the mean flow velocity (less than 1% of the local mean centerline velocity).

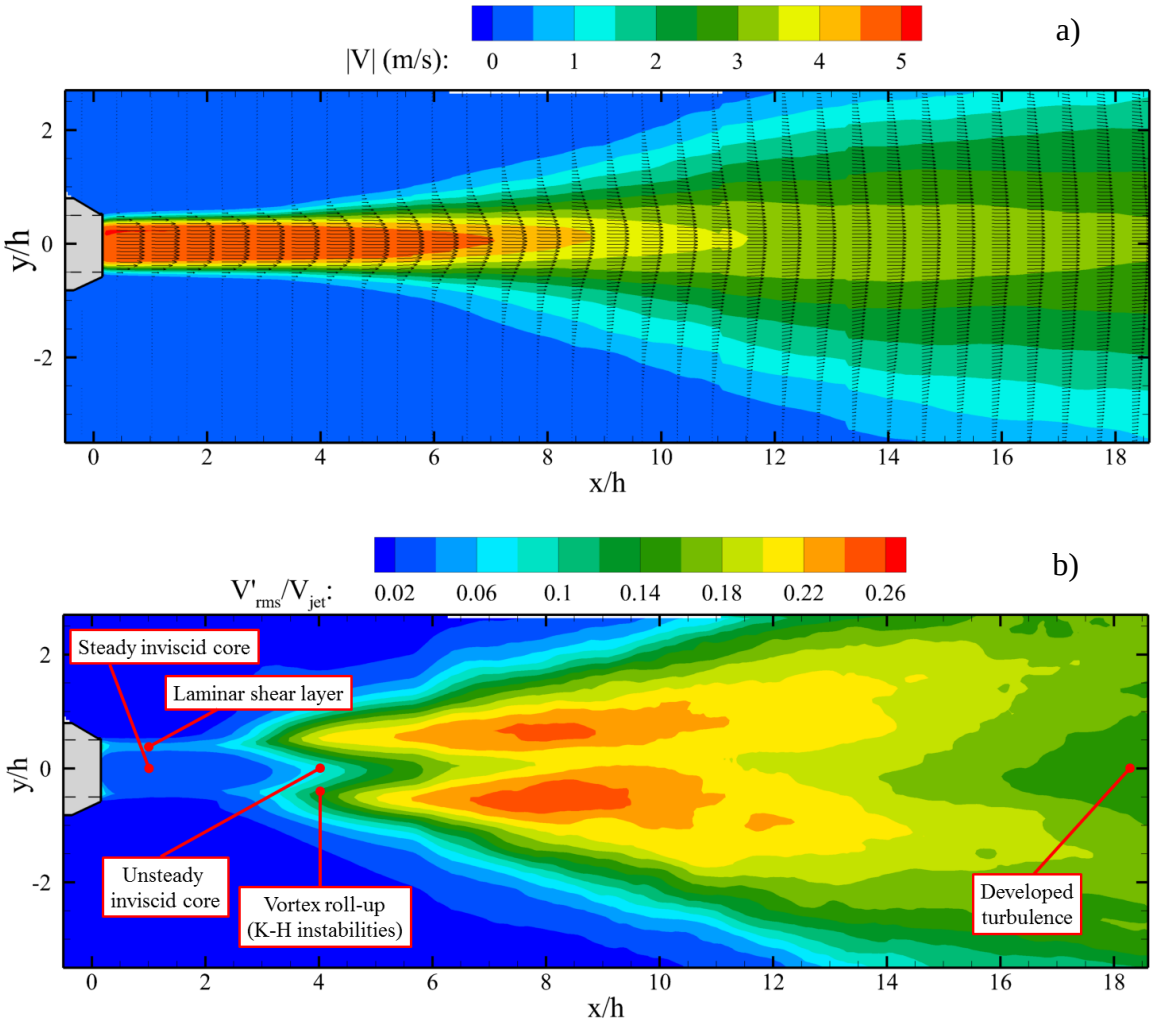

Figure 1. Time-averaged velocity (a) and fluctuations root-mean-square (b) of the jet velocity flow.

3. Mapping of the HDR velocity onto the MS coordinates

When expressed in pixel units, MS and HDR system have different coordinates. In fact, the two systems have different optical magnification factor, yielding different pixel size (i.e. the dimension in the physical space of each pixel of the image is different). We indicate with h_{MS} and h_{HDR} the pixel size of the two systems, respectively. Due to the difference in magnification factor, $h_{MS} \approx$ 3-4 h_{HDR}. Furthermore, the HDR velocity is defined in a subdomain of the MS domain (see figure 2), thus (0,0) of the HDR system corresponds to (x_0>0, y_0>0) in the MS. As a consequence, any point P has different pixel coordinates in MS and HDR systems. Therefore, a mapping function is required to map the HDR velocity fields onto the MS coordinate system. The mapping function is built using an algorithm based on the stereo self-calibration algorithm (Wieneke, 2005). Let us indicate with I_{MS} and I_{HDR} the raw images of the MS and the dewarped images of the HDR (those used in the stereo-PIV calculation), respectively. First, the images of the MS are interpolated on a grid with pixel size h_{HDR}, yielding I'_{MS}: the scaling factor of the interpolation is $s = h_{MS}/h_{HDR}$. I'_{MS} and I_{HDR} have the same pixel size. A cross-correlation is conducted between I'_{MS} and I_{HDR}: the position of the cross-correlation peak represents the shift between the origin of the two coordinate systems, which is indicated with (x_0, y_0). To enhance the peak detectability in presence of noise in the images, cross-correlation functions stemming from a set of 100 images are averaged. Thus, the mapping function that maps the HDR coordinates and velocities onto the MS is:

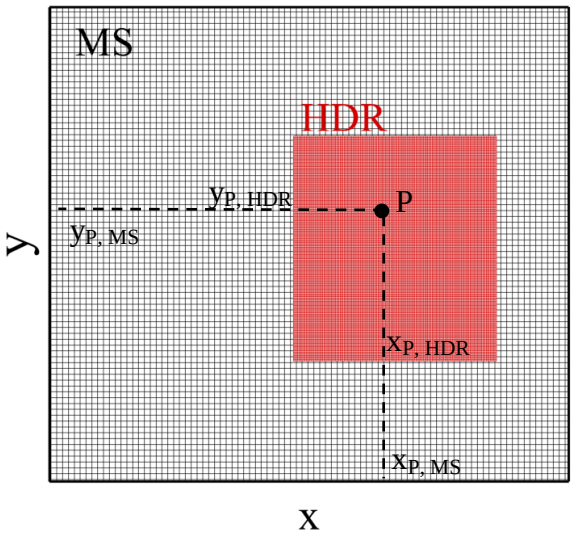

Figure 2. Comparison of HDR and MS domains.

$$\begin{cases} x'_{HDR} = x_0 + \dfrac{x_{HDR}}{s} \\ y'_{HDR} = y_0 + \dfrac{y_{HDR}}{s} \\ u'_{HDR} = \dfrac{u_{HDR}}{s} \\ v'_{HDR} = \dfrac{v_{HDR}}{s} \\ w'_{HDR} = \dfrac{w_{HDR}}{s} \end{cases} \quad (1)$$

Note that the mapping function (1) accounts for a dilatation and a shift between HDR and MS coordinates, but not for any rotation or deformation. However, since the MS camera and the HDR camera 1 were along the same line of sight and there was no relative rotation between them, no deformation or rotation between the images of the two systems is present.

Knowing the HDR coordinates and velocities (x_{HDR}, $y_{HDR,}$ $u_{HDR,}$ $v_{HDR,}$ w_{HDR}) and the mapping function parameters (x_0, y_0, s), the determination of the mapped coordinates and velocities (x'_{HDR}, $y'_{HDR,}$ $u'_{HDR,}$ $v'_{HDR,}$ w'_{HDR}) based on (1) is straightforward.

4. Format of the image and data files

Each data set of the database contains:

- The raw images of the PIV-MS.
- The reference velocity fields computed from the images of the PIV-HDR system.

The images are in 16-bit tif format and they can be read in MATLAB via the function *imread*.

The reference velocity data in ACII files with extension "*.dat*". They are in "Tecplot data" format and they can readily be loaded on Tecplot. The data files have a three-line header that indicates the title of the file, the variables name, the zone and the number of grid points along *x*- and *y*-direction (I and J, respectively).

```
TITLE = "B00004"
VARIABLES = "X", "Y", "Vx", "Vy", "Vz", "flag"
ZONE T="B00004", I=140, J=155
313 204 0.000000 0.000000 0.000000 0
314 204 0.000000 0.000000 0.000000 0
315 204 0.000000 0.000000 0.000000 0
316 204 -0.053879 -0.284982 -0.019287 1
317 204 -0.050660 -0.301307 -0.029066 1
318 204 -0.023017 -0.348236 -0.058477 1
```

Figure 3. Example of the first nine lines of a data file.

The data files contain 6 variables:

Variable	Meaning
X	Position of the grid point along the horizontal direction (in pixel units);
Y	Position of the grid point along the vertical direction (in pixel units);
u	Horizontal velocity in pixel units;
v	Vertical velocity in pixel units;
w	Out-of-plane velocity in pixel units;
flag	1 for valid vectors, 0 for invalid vectors (e.g. outside of the measurement domain.

The variables values are separated by a single space.

Note that the variables *X*, *Y*, *u*, *v*, *w* are expressed in pixel units of the measurement system (MS), so they can be directly compared with the PIV-MS velocity for the determination of the measurement error.

References

Neal DR, Sciacchitano A, Smith BL and Fulvio S (2015), Collaborative framework for PIV uncertainty quantification, Meas Sci Technol

Sciacchitano A, Scarano F, and Wieneke B (2012), Multi-frame pyramid correlation for time-resolved PIV, Exp Fluids, 53(4) 1087-1105

Timmins BH, Wilson BW, Smith BL and Vlachos PP (2012), A method for automatic estimation of instantaneous local uncertainty in particle image velocimetry measurements, Exp Fluids, 53(4) 1133-1147

Westerweel J and Scarano F (2005), Universal outlier detection for PIV data, Exp Fluids 39 1096-1100

Wieneke B (2005), Stereo-PIV using self-calibration on particle images, Exp Fluids 39 267-280

Wilson BM and Smith BL (2013), Uncertainty on PIV mean and fluctuating velocity due to bias and random errors, Meas Sci Technol, 24(3) 035302